

**QUANTITATIVE ANALYSIS OF
BRAIN WHITE MATTER
USING DIFFUSION TENSOR IMAGING**

NUR HARTINI BINTI MOHD TAIB

UNIVERSITI SAINS MALAYSIA

2014

**QUANTITATIVE ANALYSIS OF BRAIN WHITE MATTER
USING DIFFUSION TENSOR IMAGING**

by

NUR HARTINI BINTI MOHD TAIB

**Thesis submitted in fulfillment of the requirements
for the degree of
Doctor of Philosophy**

December 2014

ACKNOWLEDGEMENTS

“In the name of Allah, The Most Gracious, The Most Merciful”.

Above all, all praises to Allah SWT for giving me the strength and ability to complete this thesis. I am indebted to many people who have assisted me in this research.

First and foremost, I would like to express my deepest gratitude to my main supervisor, Assoc. Prof. Dr. Wan Ahmad Kamil Wan Abdullah and co-supervisor, Prof. Dr. Ibrahim Lutfi Shuaib. I am very grateful for their support, advice, help and guidance during my study and in the completion of this thesis.

I am particularly indebted to Dr. Enrico Magosso from Advanced Medical and Dental Institute (AMDI) as well as Prof. Dr. Yuen Kah Hay from School of Pharmaceutical Sciences. They have allowed me to take part in their project on tocotrienol vitamin E. This research would have not been a success without their effort and hard work in recruiting all the subjects with leukoaraiosis.

I have been fortunate that during the period of my study I had the opportunity to get involved in collaboration held between Universiti Sains Malaysia (USM) and foreign institutions. I am very thankful to Prof. Dr. Jafri Malin Abdullah, Head Department of Neuroscience. He had permitted me to join the Signal Processing Course conducted at his department where I met Prof. Dr. Pedro Valdés Sosa from Cuban Neuroscience Center. I really appreciate the chance to have fruitful discussions with him.

Many thanks are also dedicated to Prof. Dr. Mandava Rajeswari and all members of the Computer Vision Research Group led by her. I gained a lot when School of Computer Sciences had collaboration with Eindhoven University, Netherlands. From there, I had the opportunity to meet Prof. Dr. Bart ter Haar Romeny, Dr. Vesna Prčkovska, and Dr. Tim Peeters. They have vast experience in research on diffusion tensor imaging. I am very thankful to them and enjoyed having constructive discussions with them.

Further, I would like to express my deepest gratitude to colleagues who were most involved in this research. They are the radiographers, Mr. Mohammad Haniff Mohd Rasli,

Mrs. Noor Faizura Zainal, Mrs. Nazirah Abd Abis, and Mrs. Noor Aishah Mohd Zainal as well as the science officer, Mrs. Suzana Mat Isa. I am also very thankful to all staff at Imaging Unit, Clinical Trial Centre, AMDI. Thank you very much for the assistance afforded to me in acquiring all the data images as well as for being friends who always cheered me up during the stressful days. I am also grateful to all volunteers who have participated in the study. This research would not be accomplished without their help and cooperation.

I appreciated, as well, the support from USM and Ministry of Education Malaysia via the Academic Staff Training Scheme throughout the period of my study. This research was also funded by USM via Research University Postgraduate Research Grant Scheme (1001/PPSP/8145002).

Heartiest thanks are dedicated to my beloved husband, Muhammad Nur Salihin Yusoff, our lovely daughter, Nurul Iman and adorable son, Muhammad Adib. I am so lucky for having a husband who always understands the journey that I have to go through as both of us were striving for success throughout our Master and PhD study. I really appreciate his kind assistance, fruitful insights, and even criticism on all my works. I am very grateful to God for what He had given to me and I am very thankful to my husband and children for their love, sacrifice, support and prayers for me. They have been and will always be my source of inspiration.

I am also very thankful to my father, Mohd Taib Ariffin. He was diagnosed with rectal cancer when I was in the fifth semester of PhD study and I really hope that he will heal someday in the future. May Allah reward him strength and patience in facing all of His tests. I also thank my mother, Saniah Hanapiah, and my mother-in-law, Zawiah Mat Hussin for their prayers for both of us and for many things in life. Thanks are also due to our nice siblings and in-laws, our family members and fellow friends for their prayers, encouragement and support. Finally, thank you to any individuals who have contributed to this research either directly or indirectly. May God repay all their kindness.

TABLE OF CONTENTS

ACKNOWLEDGEMENT	ii
TABLE OF CONTENTS	iv
LIST OF TABLES	ix
LIST OF FIGURES	x
LIST OF ABBREVIATIONS	xiv
LIST OF SYMBOLS	xvi
ABSTRAK	xvii
ABSTRACT	xix
CHAPTER 1 – INTRODUCTION	
1.1 Motivation	1
1.2 Research problems	2
1.3 Objectives	4
1.4 Scope of research	4
1.5 Outline of the thesis	5
CHAPTER 2 – DIFFUSION TENSOR IMAGING AND TRACTOGRAPHY OF THE BRAIN	
2.1 Brain white matter	7
2.1.1 Axons in brain white matter	7
2.1.2 Sources of diffusion anisotropy	8
2.2 Principles of diffusion imaging	9
2.3 Principles of diffusion tensor imaging	12
2.3.1 Isotropic and anisotropic diffusion	12
2.3.2 DTI indices	14
2.4 Fibre tractography	17
2.5 Technical considerations	18
2.5.1 Trade-offs between resolution, SNR, and scan time	18
2.5.2 Diffusion encoding directions	19
2.5.3 Ratio of DWI: b_0 images	19

2.5.4	Parallel imaging	19
2.5.5	Artefacts	20
	(a) Eddy currents artefact	20
	(b) Susceptibility artefact	21
	(c) Motion artefact	21
2.6	Application of DTI in brain imaging	22
2.6.1	Leukoaraiosis	23

CHAPTER 3 – FEASIBILITY OF ACQUIRING DTI DATA AND CONSTRUCTING PARAMETRIC MAPS AND FIBRE TRACTOGRAPHY

3.1	Introduction	24
3.2	Materials and methods	24
3.2.1	Subjects	24
3.2.2	MR imaging	25
3.2.3	Image processing and fibre tracking	26
3.2.4	Region of interest and quantitative measurements	27
3.2.5	Statistical analysis	28
3.3	Results	28
3.3.1	Technical aspects	28
	(a) Image format	28
	(b) Diffusion encoding directions	29
	(c) Data sampling orientation	29
	(d) Voxel size	30
3.3.2	Assessment of leukoaraiosis and healthy brain using DTI	33
3.4	Discussions	37
3.4.1	Technical aspects	37
3.4.2	Scan time	37
3.4.3	Selection of <i>p</i> value	37
3.4.4	Comparison between leukoaraiosis and healthy white matter	38
3.4.5	Limitations and recommendations for future work	39
3.5	Conclusion	39

CHAPTER 4 – OPTIMIZATION OF DTI ACQUISITION PARAMETERS

4.1	Introduction	40
4.2	Materials and methods	42
4.2.1	Subjects	42
	(a) Phantom	42
	(b) Human volunteer	42
4.2.2	MR imaging	42
	(a) Phantom study	42
	(b) In vivo study	43
4.2.3	Data analysis	44
	(a) Measurement of signal-to-noise ratio	44
	(b) Measurement of DTI parameter indices	45
4.2.4	Statistical analysis	46
4.3	Results	46
4.3.1	Phantom study	46
4.3.2	In vivo study	49
4.4	Discussions	52
4.4.1	Imaging parameters	52
4.4.2	Assessment on SNR	53
4.4.3	ADC and FA values	54
4.4.4	Limitations and recommendations for future work	56
4.5	Conclusion	57

CHAPTER 5 – DTI MEASUREMENT OF LEUKOARAIOSIS AND NORMAL BRAIN TISSUE IN DIFFERENT BRAIN REGIONS

5.1	Introduction	58
5.2	Materials and methods	59
5.2.1	Subjects	59
5.2.2	MR imaging	61
5.2.3	Image processing and fibre tracking	62
5.2.4	Region of interest and quantitative measurements	62
5.2.5	Statistical analysis	64

5.3	Results	65
5.3.1	Inter subject variability and comparison of MD and FA between all white matter	65
5.3.2	Comparison of MD and FA between LA, NABT, and CONTROL	65
5.3.3	Comparison of MD and FA between NABT and CONTROL at various ROI	65
5.3.4	Comparison of fibre tractography of subjects with and without leukoaraiosis	69
5.4	Discussions	70
5.4.1	Inter subject variability and comparison of MD and FA between all white matter	70
5.4.2	Comparison of MD and FA between LA, NABT, and CONTROL	71
5.4.3	Comparison of MD and FA between NABT and CONTROL at various ROI	72
5.4.4	Comparison of fibre tractography of subjects with and without leukoaraiosis	73
5.4.5	Limitations	73
5.5	Conclusion	74

CHAPTER 6 – CHARACTERIZATION OF LEUKOARAIOSIS USING LESION – TO – NORMAL APPEARING WHITE MATTER RATIO

6.1	Introduction	75
6.2	Materials and methods	77
6.2.1	Subjects	77
6.2.2	MR imaging	77
6.2.3	Data analysis	78
	(a) ROI and volume measurement	78
	(b) Measurement of DTI parameter indices	78
	(c) Calculation of LNR	79
	(d) Classification of lesion size	80
	(e) Comparison between “many small” and “few big”	80
6.2.4	Statistical analysis	81
6.3	Results	81

6.3.1	Characterization of leukoaraiosis and NAWM using MD and FA	81
6.3.2	Characterization of leukoaraiosis using LNR	83
6.3.3	Association of MD, FA, and LNR with volume of leukoaraiosis	83
6.3.4	Intra- and inter-individual variability of LNR	85
	(a) Intra-individual variability	85
	(b) Inter-individual variability	85
6.3.5	Comparison between “many small” and “few big”	88
6.4	Discussions	91
6.4.1	The outliers	91
6.4.2	Characterization of leukoaraiosis and NAWM using MD and FA	92
6.4.3	Characterization of leukoaraiosis using LNR	92
6.4.4	Association of MD, FA, and LNR with volume of leukoaraiosis	93
6.4.5	Comparison between “many small” and “few big”	95
6.5	Conclusion	96
CHAPTER 7 – SIGNIFICANCE OF THE STUDY, CONCLUSION AND FUTURE RECOMMENDATIONS		
7.1	Significance of the study	98
7.2	Conclusion	99
7.3	Recommendations for future work	101
REFERENCES		103
APPENDIX		117
LIST OF PUBLICATIONS		118

LIST OF TABLES

		Page
Table 3.1	List of diffusion gradient vectors applied for each volume of data images.	31
Table 4.1	Imaging parameters which were kept fixed for all protocols.	43
Table 4.2	Imaging parameters that were altered according to six protocols assessed.	44
Table 5.1	Some studies comparing DWI/ DTI values of leukoaraiosis, normal appearing brain tissue, and normal brain tissue.	60
Table 5.2	Demographic data of participating subjects.	61
Table 5.3	Intersubject variability of MD and FA values obtained from CONTROL subjects.	67
Table 5.4	MD and FA values of LA, NABT, and CONTROL at frontal and occipital white matter.	68
Table 6.1	Summary of MD and FA values measured at all ROIs.	82
Table 6.2	Description of lesions volume, LNR, and DTI values.	89

LIST OF FIGURES

		Page
Figure 2.1	Structure of (a) a neural cell (Brookshire, 2006) and (b) the cytoskeleton within the axon that hinders diffusion perpendicular to the axonal membrane and facilitates parallel diffusion i.e. along the axon (Beaulieu, 2009, p. 107).	8
Figure 2.2	Schematic diagram of the Stejskal-Tanner sequence added to spin echo EPI sequence. The dotted lines denote continuation of the sequence for subsequent repetition time, TR (Modified from Alexander et al., 2007, p. 318).	11
Figure 2.3	Illustration of isotropic and anisotropic diffusion (Winston, 2012, p. 258)	14
Figure 2.4	An example of b_0 , principle diffusivities ($\lambda_1, \lambda_2, \lambda_3$), Trace (\mathbf{D}), radial diffusivity (D_{\perp}), MD, and colour coded FA maps as obtained from this work.	16
Figure 2.5	An example of fibre tractography overlaid on colour-coded FA map. The images depict two main fibre bundles in the white matter such as (a) corpus callosum and (b) cerebrospinal tract from left sagittal view.	18
Figure 2.6	Parallel reconstruction of data in which images with aliasing artefacts are obtained simultaneously. The data are then combined to obtain a complete image (centre) (Clarke, 2007).	20
Figure 3.1	Three square ROIs were drawn in right and left 1) frontal white matter, 2) genu, 3) caudate nucleus, 4) lentiform nuclei, 5) thalamus, 6) splenium, 7) occipital white matter, 8) occipital grey matter, 9) cerebrospinal fluid, and 10) centrum semiovale.	27
Figure 3.2	Multiplanar presentation of DTI maps ^a with (a) wrong and (b) correct fibre orientation. (c) Fibre tractography ^b of the same dataset in (a) produced wrong tractography and could be seen obviously in corpus callosum fibre bundles (arrow). Fig. (d) and (e) were obtained from the same dataset shown in (b).	32
	^a DTI maps acquired using MedInria software ^b Fibre tractography images in (c) and (d) was obtained using DTI Tool while that in (e) was obtained using TrackVis software.	
Figure 3.3	Posterior coronal view of fibre tractography ^a gained from data images acquired using (a) nonisotropic and (b) isotropic voxel size.	33
	^a Performed using NordicICE software.	

Figure 3.4	T2-weighted images, ADC maps, and FA maps of normal brain (a-c) and brain with leukoaraiosis (d-f). The arrows show the area of leukoaraiosis in the occipital white-matter region. Note the bright appearance of leukoaraiosis in ADC map, showing high diffusivity (e), whereas low anisotropy was observed in the FA map (f).	34
Figure 3.5	Fiber tractography of (a) normal and (b) leukoaraiosis subjects at occipital lobes. Note the obvious discontinuity of 1) pcr/cpt/ifo/ilf/ptr ^a and 2) forceps major tracts [indicated by yellow dashed lines in (a)] on right and left hemispheres in (b).	34
	^a pcr: posterior corona radiata, cpt: corticopontine tract, ifo: inferior fronto-occipital fasciculus, ilf: inferior longitudinal fasciculus, ptr: posterior thalamic radiation	
Figure 3.6	ADC, trace, and FA values at all ROIs ^a for normal and leukoaraiosis subjects. Areas which show significant difference ($p < .01$) between subjects are indicated by red asterisk.	35
	^a fWM: frontal white matter, Sp: splenium, cNuc: caudate nucleus, lNuc: lentiform nucleus, Thal: thalamus, oWM: occipital white matter, oGM: occipital grey matter, CSF: cerebrospinal fluid, CS: centrum semiovale.	
Figure 4.1	SNR of phantom for specific combination of voxel size and b-value. All except protocols V2.0 B1200 and V2.0 B1000 displayed $SNR \geq 20$. The error bars indicate standard deviation between three measurements.	47
Figure 4.2	An example of DWI of phantom produced by all protocols during DTI scan at similar diffusion encoding direction, i.e. (1,0,0).	48
Figure 4.3	Mean and standard deviation of ADC and FA value measured on phantom images. A remarkably high standard deviation, thus variance (σ^2) was noted in V2.0 B1200.	48
Figure 4.4	SNR measured at WM, GM, and CSF areas of human brain. Sufficient SNR at CSF was noticed for all protocols. It can be seen that voxel size of $2.5 \times 2.5 \times 2.5 \text{ mm}^3$ demonstrated higher SNR than voxel size of $2.0 \times 2.0 \times 2.0 \text{ mm}^3$ for the three areas.	49
Figure 4.5	ADC ^a and FA values at all ROIs ^b acquired for all protocols. Results from this study were compared with that of obtained from previous studies ^c . Note that V2.5 B1000 and V2.5 B700 show smallest deviation of ADC and FA values from previous findings.	51
	^a ADC reported as MD in some of the articles referred. ^b fWM: frontal white matter; Sp: splenium; cNuc: caudate nucleus; lNuc: lentiform nucleus; Thal: thalamus; oWM: occipital white matter; oGM: occipital grey matter. ^c Ref-highest: highest values in reference, Ref-lowest: lowest values in reference, This study: values obtained in this study.	
Figure 4.6	Percentage of difference of (a) ADC and (b) FA values obtained in this study as compared to references. Bars show differences at each ROI for all protocols. Values that matched with previous studies are indicated as 0% differed from references.	52

Figure 5.1	An example of ROIs placement on subjects with leukoaraiosis. ROIs were identified on FLAIR image (a). Measurement of parameter indices was performed on the corresponding location on MD map (b). Red ROI represents LA, while NABT ROIs are shown in green.	64
Figure 5.2	(a) MD and (b) FA values at white matter and grey matter region for NABT and CONTROL. No significant different was noted between the two categories.	68
Figure 5.3	Fibre tractography obtained from two subjects exhibiting the corpus callosum (red anatomy pointed by arrow) from left sagittal view. Shown are the anterior [(a) and (d)], posterior [(b) and (e)], and superior [(c) and (f)] callosal fibres. Number of fibres (n_f) in those areas are as displayed. Colour indicates fibre direction as follows: red: R-L, green: A-P, and blue: S-I.	69
Figure 6.1	An example of ROI placement on FLAIR images of subject with a) big lesions and b) small lesions. ‘L’ ROIs are represented by yellow freehand ROI while ‘N’ ROIs are represented by green circle located near to the lesion. In (b), some ‘N’ ROIs (labelled 1, 2, and 3) correspond to multiple ‘L’ ROIs (marked with asterisks).	80
Figure 6.2	Distribution of MD and FA of leukoaraiosis (LA) and NAWM for all 274 ROI data obtained from 49 subjects. ^a The dropping of the two outliers in the graph above did not change the regression line.	82
Figure 6.3	Distribution of LNR versus FA of leukoaraiosis for all 274 ROI data ^a obtained from 49 subjects. ^a The dropping of the two outliers in the graph above did not change the regression line.	83
Figure 6.4	Graphs showing correlation and regression ^a between (a) LNR and leukoaraiosis volume ^b , (b) MD and leukoaraiosis volume, and (c) FA and leukoaraiosis volume. ^a The dropping of the two outliers in (a) and (b) did not change the regression line. ^b Volumes are displayed in Log ₅ scale.	84
Figure 6.5	(a) MD values of leukoaraiosis (LA) and NAWM measured at 19 ROIs identified in the brain of single patient. (b) LNR and FA values for each ROI. Displayed at base of bars are the ROI volumes in cm ³ . High LNR and low FA value indicates considerable tissue damage.	86
Figure 6.6	Graphs showing LNR and FA values (upper row) and MD values (bottom row) for leukoaraiosis (LA) and NAWM tissues. Both charts in the left column represent Subject 1, at centre are that of Subject 2, and right column are that of Subject 3. Displayed at base of bars are volumes of each ROI in cm ³ .	87

Figure 6.7	(a) LNR and (b) FA of leukoaraiosis ROIs measured from twelve subjects. Number of small (S), medium (M), and large (L) lesions ^a in each subject (S1 to S12) are displayed in the legend.	90
	^a Volumes are displayed in Log ₁₀ scale.	
Figure 6.8	(a) Association of LNR and FA for both groups and (b) 3-dimensional presentation of LNR, FA, and lesion volume measured from subjects in “many small (MS)” and “few big (FB)” groups. A weak negative association was found only between LNR and FA in “many small” group.	91

LIST OF ABBREVIATIONS

AC	Anterior commissure
ACF	Anterior callosal fibres
ADC	Apparent Diffusion Coefficient
ASSET	Array Spatial Sensitivity Encoding Technique
A-P	Anterior - Posterior
CSF	Cerebrospinal fluid
CV	Coefficient of variation
DED	Diffusion encoding direction
DICOM	Digital Imaging and Communications in Medicine
DWI	Diffusion-Weighted Imaging
DTI	Diffusion Tensor Imaging
EPI	Echo Planar Imaging
FA	Fractional Anisotropy
FACT	Fibre assignment by continuous tracking
FLAIR	Fluid Attenuated Inversion Recovery
FOV	Field of view
GM	Grey matter
LA	Leukoaraiosis
LNR	Lesion-to-Normal appearing white matter Ratio
MD	Mean Diffusivity
MRI	Magnetic Resonance Imaging
NABT	Normal Appearing Brain Tissue
NAWM	Normal Appearing White Matter
NEX	Number of signal averaging
NifTI	Neuroimaging Informatics Technology Initiative
NVA	Neurovascular array
PC	Posterior commissure
PCF	Posterior callosal fibres
PD	Proton density
RA	Relative Anisotropy
RBW	Receiver Bandwidth
RF	Radio Frequency
RGB	Red Green Blue

ROI	Region of interest
R-L	Right - Left
SAR	Specific absorption rate
SD	Standard deviation
SCF	Superior callosal fibres
SNR	Signal-to-Noise Ratio
S-I	Superior - Inferior
SS-EPI	Single shot - Echo Planar Imaging
T1	Longitudinal relaxation time
T2	Transversal relaxation time
TE	Echo time
TR	Repetition time
VR	Volume ratio
WM	White matter

LIST OF SYMBOLS

δ	Duration of diffusion gradient (ms)
Δ	Period between the start of the diffusion gradient before and that after a 180° pulse (ms)
γ	Gyromagnetic ratio (MHz/T)
$\lambda_1, \lambda_2, \lambda_3$	Eigenvalues of the diffusion tensor
σ^2	Variance
ΔZ	Slice thickness
b	b-value, a scalar characterizing the diffusion sensitizing gradient (s/mm ²)
D	Diffusion coefficient (mm ² /s)
D_{\parallel}	Axial diffusivity (mm ² /s)
D_{\perp}	Radial diffusivity (mm ² /s)
\mathbf{D}, \mathbf{D}'	Diffusion tensor
g	g-factor in parallel imaging technique
G	Amplitude of diffusion gradient (mT/m)
G_x, G_y, G_z	Diffusion gradient in x-, y-, and z-directions, respectively
N_x, N_y	Number of frequency- and phase-encoding matrix, respectively
R	Acceleration factor used during acquisition using parallel imaging technique ($R \geq 1$)
S, S_0	Signal intensities with and without diffusion-weighting, respectively
$\mathbf{v}_1, \mathbf{v}_2, \mathbf{v}_3$	Eigenvectors that correspond to each $\lambda_1, \lambda_2,$ and $\lambda_3,$ respectively
X_f, X_h, X_l	ADC and FA values measured in current study, that the highest value from reference, and that the lowest value from reference, respectively.

ANALISIS KUANTITATIF JIRIM PUTIH OTAK MENGUNAKAN PENGIMEJAN TENSOR DIFUSI

ABSTRAK

Penyelidikan ini mengenai aplikasi pengimejan tensor difusi (DTI) dalam kajian tentang leukoaraiosis dan jirim putih normal. Empat objektif utama yang telah digariskan dalam kajian ini telah tercapai. Sebuah fantom kepala telah digunakan dan sejumlah 15 subjek normal dan 51 subjek leukoaraiosis telah mengambil bahagian dalam kajian ini. Sejumlah 5128 hirisan telah dianalisis dalam kerja ini. Pengimejan otak telah dijalankan menggunakan sistem pengimejan resonan magnet (MRI) 1.5 Tesla.

Keupayaan mendapatkan data DTI dan membina trektografi gentian untuk kajian leukoaraiosis telah dikaji. Hasil yang didapati menunjukkan kebolehan DTI untuk membezakan leukoaraiosis daripada jirim putih normal. Trektografi gentian telah menunjukkan perbezaan struktur yang jelas bagi gentian saraf dalam kawasan jirim putih. Dapat disimpulkan data DTI dan pembinaan trektografi gentian untuk penilaian leukoaraiosis didapati boleh dilaksanakan.

Gabungan optimum peleraian saiz voksel dan nilai b untuk pengimejan seluruh otak juga telah dapat ditentukan. Enam protokol yang terdiri daripada gabungan pelbagai saiz voksel dan nilai b telah dinilai. Pengukuran nisbah isyarat-hingar (SNR) dan indeks parameter DTI telah dijalankan bagi kedua-dua kajian fantom dan in vivo. Protokol dengan saiz voksel $2.5 \times 2.5 \times 2.5 \text{ mm}^3$ telah didapati memberikan nilai SNR yang diperlukan, iaitu sekurang-kurangnya 20. Gabungan parameter yang optimum ialah saiz voxel $2.5 \times 2.5 \times 2.5 \text{ mm}^3$ dengan nilai b 700 s/mm^2 .

Penilaian leukoaraiosis (LA) di dalam kawasan yang berbeza menggunakan nilai-nilai difusi min (MD) dan anisotropi pecahan (FA) telah dijalankan. Nilai MD dan FA telah dibandingkan dengan tisu otak yang kelihatan normal (NABT) yang diukur daripada subjek leukoaraiosis dan tisu otak normal (CONTROL) yang diukur daripada subjek kawalan yang sihat. LA didapati menunjukkan nilai-nilai MD lebih tinggi dan FA lebih rendah secara signifikan berbanding NABT pada kawasan jirim putih frontal dan oksipital. Tiada perbezaan ditemui bagi MD dan FA antara NABT dan CONTROL pada semua kawasan jirim putih dan kelabu. Daripada kajian trektografi gentian, didapati bahawa terdapat pengurangan yang besar jumlah gentian saraf subjek leukoaraiosis berbanding subjek normal.

Pencirian leukoaraiosis telah dijalankan menggunakan nisbah lesi-jirim putih yang kelihatan normal (LNR). Kaedah ini dicadangkan buat kali pertama. Satu pendekatan baru yang lain ialah pengukuran isipadu lesi pada setiap tempakan lesi secara khusus. Perkaitan antara LNR dan isipadu lesi didapati tiada kaitan antara keduanya. Di sini dicadangkan bahawa tahap kerosakan tisu tidak berkait dengan saiz lesi.

QUANTITATIVE ANALYSIS OF BRAIN WHITE MATTER USING DIFFUSION TENSOR IMAGING

ABSTRACT

This research is concerned with the application of diffusion tensor imaging (DTI) in the study of leukoaraiosis and normal white matter. Four main objectives outlined in the study have been achieved. A head phantom was used and a total of 15 normal subjects and 51 leukoaraiosis subjects participated in the study. A total of 5128 slices were analysed in this work. Brain imaging was performed using 1.5 Tesla MRI system.

Feasibility of acquiring DTI data and constructing fiber tracts for leukoaraiosis study was investigated. Results obtained showed capability of DTI to distinguish leukoaraiosis from normal white matter. Fiber tractography exhibited a good structural differentiation of nerve fibers in the white matter region. Acquiring DTI data and constructing fiber tractography for assessment of leukoaraiosis was found to be feasible.

Optimum combination of voxel size resolution and b-value for the whole brain imaging has also been determined. Six protocols which consist of the combination of various voxel size and b-value were evaluated. Measurement of signal-to-noise ratio (SNR) and DTI parameter indices was carried out for both phantom and in-vivo studies. It was found that protocols with voxel $2.5 \times 2.5 \times 2.5$ mm³ give the desired SNR of at least 20. The optimal combination of parameters are the voxel size of $2.5 \times 2.5 \times 2.5$ mm³ with b-value of 700 s/mm².

Assessment of leukoaraiosis (LA) at different region in the brain using mean diffusivity (MD) and fractional anisotropy (FA) values were carried out. The MD

and FA values were compared with that of measured at normal appearing brain tissue (NABT) from leukoaraiosis subjects and normal brain tissue (CONTROL) from healthy subjects. It was found that LA demonstrated a significantly higher MD and lower FA as compared to NABT in frontal and occipital white matter areas. No differences were noted in MD and FA with regard to all white and grey matter regions between NABT and CONTROL categories. From fibre tractography it was also found that there is major reduction in the number of neural fibres in leukoaraiosis subject as compared to normal subject.

Characterization of leukoaraiosis was performed using lesion-to-normal appearing white matter ratio (LNR). This method is proposed for the first time. Another new approach is measurement of lesion volume at each specific lesion spot. Correlation between LNR and lesion volume indicated that LNR is not associated with the lesion volume. Therefore, it is suggested that the degree of tissue destruction is not associated with size of the lesion.

CHAPTER 1

INTRODUCTION

1.1 Motivation

The advent of advanced magnetic resonance imaging (MRI) techniques, particularly diffusion imaging has opened up new vista for more research to be done in order to understand how human brain works. Diffusion weighted imaging (DWI), subsequently diffusion tensor imaging (DTI) is an MRI technique that detects and measures mobility of water molecules in biological cells. DWI is the conventional technique in diffusion imaging in which it measures the mobility of water molecules in only one direction. While DTI is the advanced technique that measures the mobility of water molecules in many directions and at least in the three orthogonal planes i.e. x, y, and z. The physical basis underlying diffusion imaging techniques is described in detail in Chapter 2.

The advantage of DTI over the other conventional MRI techniques is that it offers useful quantitative information via its specific parameter indices. Such parameter includes mean diffusivity (MD) which gives information on the degree of movement of water molecules at a region of interest, and fractional anisotropy (FA) which quantifies the degree of directionality of water movement at that particular region. Also, a unique advantage of DTI is that it allows reconstruction of cerebral nerve fibre tracts through a method called fibre tractography. Via fibre tractography method, visualization of the cerebral nerve fibres is available noninvasively. The emergence of this specific technique permits better understanding of brain neural

architecture thus aids in investigation of various brain and especially neurological diseases.

At Advanced Medical and Dental Institute University Sains Malaysia (AMDI – USM), a pharmacological study on white matter lesion, specifically leukoaraiosis has been carried out. Researchers assessed the neuroprotective effects of tocotrienol vitamin E intake on leukoaraiosis. Evaluation of lesions progression was carried out using standard MRI protocols (Magosso, 2012). In the current study, DTI is used for the assessment of leukoaraiosis. The assessment includes characterization of leukoaraiosis at specific region using information derived from DTI maps. Fibre tractography was also performed to investigate the structure of several nerve fibres at leukoaraiosis region. It is hoped that all information obtained in this study will be able to provide new insights into the condition of normal white matter and leukoaraiosis tissue in human brain.

1.2 Research problems

Since DTI is rather new in Malaysia, feasibility of acquiring DTI data using 1.5 T MRI system and constructing the parametric maps and fibre tractography need to be investigated. Furthermore, the capability of the MRI system to produce results that could distinguish leukoaraiosis from healthy white matter also needs to be evaluated.

Subsequently, since there are no standard DTI protocols, optimization of imaging protocols is necessary to ensure the acceptability of results. Optimal imaging parameters need to be determined where the particular parameters will then be used for new DTI scans and assessments of leukoaraiosis quantitatively.

As a matter of fact, MD values are quite similar between different regions in the normal human brain. However, FA varies across different regions due to different nerve fibre architecture in the brain. Therefore, assessment of leukoaraiosis must take into account the region where the leukoaraiosis is located. In the next part of this study, DTI parameter values are measured at leukoaraiosis areas as well as normal appearing white matter (NAWM) at various regions in the brain.

Since the growth of leukoaraiosis is influenced by various risk factors and mechanisms, it is assumed that severity of tissue damage at different region is not similar, therefore giving various DTI values for different lesions across the brain.

Severity of leukoaraiosis is normally assessed using visual rating scale based on the degree and distribution of the lesions (Fazekas et al., 1987; Scheltens et al., 1993; Manolio et al., 1994; Scheltens et al., 1998; Wahlund et al., 2001; Pantoni et al., 2002). Some studies defined severity based on volumetric assessment (Silbert et al., 2008; Wright et al., 2008; Rossi et al., 2010). However, a question rose concerning whether total volume really represents the real condition of tissue destruction (Ropele et al., 2009). In the final part of the study, characterization of leukoaraiosis is done using lesion-to-normal appearing white matter ratio (LNR) index in which level of tissue destruction is assessed by comparing the MD values at leukoaraiosis region with the normal tissues within the same brain. This study will analyse the correlation between LNR and size of lesion and to investigate white matter integrity in brain with many small lesions and those with few big lesions.

1.3 Objectives

The specific objectives of the study are:

- i. To evaluate the feasibility of acquiring DTI data using 1.5 T MRI and constructing the parametric maps and fiber tractography. It is also to determine the optimal DTI image acquisition parameters for the whole brain imaging.
- ii. To assess leukoaraiosis at different region in the brain using MD and FA values as well as to compare those values with that of measured in normal appearing brain tissue from leukoaraiosis subjects and normal brain tissue from healthy control subjects.
- iii. To characterize leukoaraiosis at specific lesion spot using LNR and to correlate the findings with lesion volume. It is also to compare LNR of each lesion spot in subjects with many small lesions with that of few big lesions.

In general, many aspects of DTI technique need to be explored extensively in imaging of brain white matter. The outcome of this study is expected to provide better comprehension on human white matter, particularly leukoaraiosis, which is believed to be precursor to a disease (Kuller et al., 2004; Smith et al., 2010), and hence will help in better diagnosis and prognosis of the abnormality.

1.4 Scope of research

This study focused mainly on the technical aspects of DTI. Exploration of this new tool encompassed evaluation of the capability of the MRI scanner itself as well as the acquisition parameters that may influence the image quality. Second major focus of this study is on quantitative analysis of brain white matter and leukoaraiosis. The

main interest of this research is to assess the condition of the white matter using DTI parameter indices, i.e. MD and FA and comparing it with normal brain tissue. This study tried to assess specifically each lesion spot in every individual subject and the quantitative values measured from them. In order to evaluate the degree of tissue destruction, LNR is used. Correlation between LNR with leukoaraiosis volume was also examined. However, correlating the parameter indices with the visual rating scale, which is normally done on fluid attenuated inversion recovery (FLAIR) image or any cognitive performance assessment scale is not included in this study.

1.5 Outline of the thesis

This thesis is organized according to its four specific objectives, as explained below:

Chapter 2 describes the physical and biological basis underlying diffusion imaging. In this chapter, the physical principles of diffusion imaging are explained in details. Brief information on the brain white matter, specifically the axons is also covered.

The first part of the thesis, which encompasses the work on technical aspects are presented in **Chapters 3** and **4**. These two chapters represent the first objective of the thesis. **Chapter 3** elaborates the work on feasibility study while **Chapter 4** presents the work on optimization of the image acquisition parameters. In this chapter, the influence of either MRI or DTI-specific acquisition parameters on DTI image quality and its parametric maps is described in depth.

The second part of this thesis, which comprises the work on quantitative analyses are included in **Chapters 5** and **6**. In **Chapter 5**, DTI measurement of

leukoaraiosis and normal white matter at various brain regions are explained rather comprehensively. **Chapter 5** corresponds to the third objective of the thesis whereas **Chapter 6** covers the final objective. **Chapter 6** describes the work on assessment of degree of tissue destruction using LNR and their association with the lesion volume. White matter integrity in subjects with many small lesions as compared to those with few big lesions are evaluated and described thoroughly in this particular chapter. Finally, **Chapter 7** presents the significance of this study, conclusion, and recommendation for future work.

CHAPTER 2

DIFFUSION TENSOR IMAGING AND TRACTOGRAPHY OF THE BRAIN

2.1 Brain white matter

2.1.1 Axons in brain white matter

Human brain is one of the most important structures in the central nervous system (CNS). It comprises of mainly a thick layer of neural tissues called cerebrum or cerebral cortex. Two main structures that form the cerebral cortex are grey matter and white matter. Besides, there are about 100 billion neurons in the cerebral cortex.

A neuron consists of its cell body, axon, as well as axon terminals and dendrites as neurotransmitter and receiver, respectively as depicted in Fig. 2.1 (a). The neuron's cell body lies in the grey matter area whereas its axon and the glial cells are in the white matter area. Axons are in size of as short as one millimetre to as long as more than one metre long, enabling them to play an important role in connecting different areas of the brain and various parts in the whole CNS ("Nervous system", 2014).

Furthermore, axons also remain in parallel arrangement and close to each other forming nerve fibre bundles. These fibre bundles are mostly organized in one direction connecting various parts of the white matter areas e.g. corpus callosum fibre bundles connecting right and left cerebral hemispheres (Wakana et al., 2004), or cingulum fibre bundle that connects the frontal lobe with the precuneus, posterior cingulate cortex, hippocampus, and parahippocampus (van den Heuvel et al., 2008). The organized formation of the nerve fibre bundles is the main factor that determines

diffusion anisotropy i.e. the directional movement of molecular diffusion in the white matter.

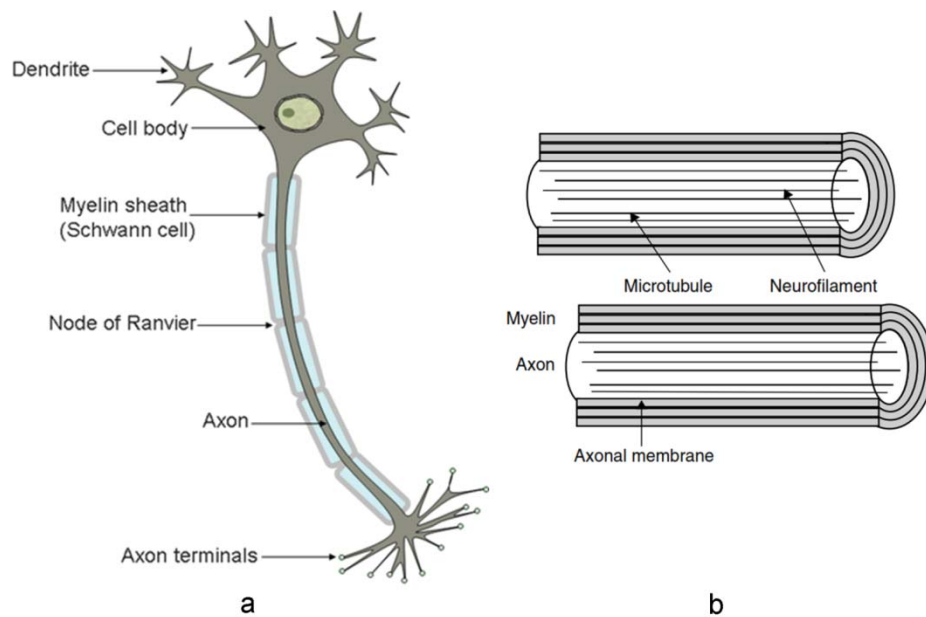


Fig. 2.1 Structure of (a) a neural cell (Brookshire, 2006) and (b) the cytoskeleton within the axon that hinders diffusion perpendicular to the axonal membrane and facilitates parallel diffusion i.e. along the axon (Beaulieu, 2009, p. 107).

2.1.2 Sources of diffusion anisotropy

It has been reported elsewhere that in the grey matter diffusion is mainly “isotropic” i.e. water molecules moves randomly, while in the white matter, on the other hand, it was found mostly “anisotropic” i.e. water tend to move in a particular direction (Winston, 2012; Moseley et al., 1990). Sources of diffusion anisotropy were believed to be due to several factors particularly axonal membranes and its diameter, Myelin sheath, and cytoskeleton (Beaulieu, 2009).

Diameter of axons is typically in range of 0.2 to 20 μm and varies between myelinated and unmyelinated axons. It was also described that anisotropy also occurs in unmyelinated axons suggesting that the axonal membranes itself contribute to

anisotropic diffusion. Furthermore, the diameter and proportion of myelinated axons also influence the axonal packing densities (Winston, 2012; Beaulieu, 2009; Edgar and Griffiths, 2009).

Within the axons are submicroscopic structures called cytoskeleton (Fig. 2.1 b). Cytoskeleton comprises of microtubules, microfilaments, and neurofilaments, each of which are in diameter sizes of nanometer (nm). These structures contribute to anisotropy by means of hindering perpendicular diffusion and facilitating parallel diffusion (Winston, 2012; Beaulieu, 2009; Edgar and Griffiths, 2009).

Besides that, axons in the CNS are enveloped by Myelin sheath, a cover made up of multiple layers of alternating lipid and protein structures. Myelin goes through some significant changes over the long-term of age (Edgar and Griffiths, 2009; Wozniak and Lim, 2006; Barkovich, 2000). Additionally, Myelin sheath also influences diffusion via its varying thickness and density contributing to different degree of hindrance to perpendicular diffusion (Winston, 2012; Beaulieu, 2009; Gulani et al., 2001).

2.2 Principles of diffusion imaging

Diffusion images are usually acquired using Stejskal-Tanner sequence or also known as pulsed gradient spin echo method. The sequence is added to spin echo EPI sequence in which data images are acquired from single echo train, hence permits very fast data acquisition (Fig. 2.2). In single-shot EPI for example, series of images could be obtained after sending in only a single radio frequency (RF) pulse (Poustchi-Amin et al., 2001; McRobbie et al., 2006a).

Using Stejskal-Tanner sequence, 90° and 180° RF pulses are applied and a symmetric pair of equal diffusion sensitizing gradient pulses is sent in on both sides of the 180° refocusing pulse (Fig. 2.2). If there is no water movement during and between the two gradients, the proton spins rephase completely. Conversely, if water molecules move, an incomplete rephasing of proton spins causes the echo amplitude to be attenuated exponentially, thus signal loss occurs. Then, the diffusion constant is measured from the amount of signal loss (Roberts and Schwartz, 2007; Mukherjee et al. 2008a; Mohd Taib, 2010).

Signal intensity at each pixel is weighted by proton density, longitudinal relaxation time ($T1$), transversal relaxation time ($T2$), and diffusion properties of water molecules in the pixel (Mori, 2007a). Suppose a very long repetition time (TR) is used, thus $T1$ weighting is negligible therefore the signal intensity of the image is described by Eq. 2.1:

$$S = PD e^{-TE/T2} e^{-bD} \quad (2.1)$$

where S is the signal intensity of the image, PD is the proton density, TE is echo time, and $T2$ is transversal relaxation time. By simplifying the term $PD e^{-TE/T2}$ as S_0 , the signal attenuation could be described as:

$$S = S_0 e^{-bD} \quad (2.2)$$

where S and S_0 are the signal intensities with and without diffusion-weighting, respectively. Signal intensities without diffusion-weighting, i.e. $b \approx 0$ s/mm^2 is also called $T2$ -weighted images or nondiffusion-weighted images or b_0 images. D is the diffusion coefficient (in mm^2/s) and b is the b-value (in s/mm^2) (Mori, 2007a). b-value is a scalar characterizing the diffusion sensitizing gradient applied during the scan and is depicted via Eq. 2.3.

$$b = \gamma^2 G^2 \delta^2 (\Delta - \delta/3) \quad (2.3)$$

where γ is the gyromagnetic ratio (42.57 MHz/T for Hydrogen protons), G is the amplitude of the diffusion gradient (in mT/m), δ is the duration of the gradient and Δ is the period between the start of the diffusion gradient before and that after the 180° pulse. δ and Δ are measured in millisecond (ms). Typically, gradient in z-direction, G_z (superior-inferior) is the slice selection gradient whereas that in y-direction, G_y (anterior-posterior) is the phase-encoding gradient, and that in x-direction, G_x (left-right) is the readout gradient. The diffusion gradient, G can be applied along any directions or combination of directions x, y, and z (Fig. 2.2).

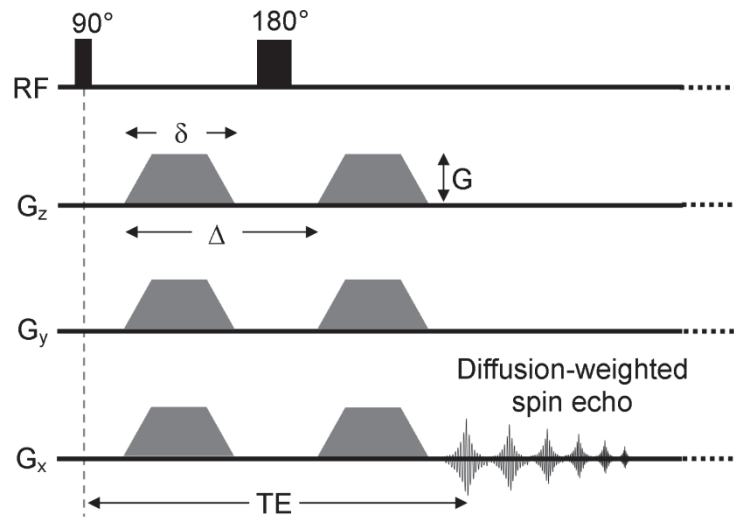


Fig. 2.2 Schematic diagram of the Stejskal-Tanner sequence added to spin echo EPI sequence. The dotted lines denote continuation of the sequence for subsequent repetition time, TR (Modified from Alexander et al., 2007, p. 318).

In Eq. 2.1, the diffusion coefficient, D characterizes the average area that protons diffuse per unit time, for example self-diffusion of pure water at room temperature is $2.299 \times 10^{-3} \text{ mm}^2/\text{s}$ (Holz et al., 2000). However, the diffusion coefficient is termed as Apparent Diffusion Coefficient (ADC) which takes into account the complexity of diffusion process in biological tissues (Moseley et al,

1990; Luypaert et al., 2001). The ADC values could be measured by acquiring two sets of images, specifically one with low b-value while another set with high b-value, i.e. the diffusion-weighted images. By fitting the respective b-value into Eq. 2.2 yields:

$$S_1 = S_0 e^{-b_1 D} \quad (2.4)$$

$$S_2 = S_0 e^{-b_2 D} \quad (2.5)$$

Ratio of Eq. 2.5 over Eq. 2.4 produces:

$$\frac{S_2}{S_1} = e^{(b_1 - b_2)D} \quad (2.6)$$

Then, solving for D gives:

$$D = \frac{1}{b_1 - b_2} \ln \frac{S_2}{S_1} \quad (2.7)$$

2.3 Principles of diffusion tensor imaging

2.3.1 Isotropic and anisotropic diffusion

The coefficient D shown in Eq. 2.7 represents “isotropic diffusion” in which water molecules moves evenly (in random and incoherent motion) in any directions. In this case, diffusion gradient could be applied in any direction as the ADC of molecules is similar at all directions. Conversely, in a highly organized structure like neural fibre bundles in the brain white matter, diffusion of water molecules to direction perpendicular to the fibres pathway is hindered by cellular membranes. This type of diffusion is called “anisotropic diffusion” which represents restricted mobility of water molecules in a preferential direction that is along the fibres. In this occasion,

diffusion gradient has to be applied in more than one direction in order to describe the anisotropic diffusion.

One way to characterize the anisotropic diffusion is by using tensor operation (Basser et al., 1994). In this mathematical model, ADC in three-dimensional space is defined as:

$$\mathbf{D} = \begin{bmatrix} D_{xx} & D_{xy} & D_{xz} \\ D_{yx} & D_{yy} & D_{yz} \\ D_{zx} & D_{zy} & D_{zz} \end{bmatrix} \quad (2.8)$$

where \mathbf{D} is the diffusion tensor while x , y , and z are the three orthogonal axes.

Diagonalization of Eq. 2.8 yields:

$$\mathbf{D}' = \begin{bmatrix} \lambda_1 & 0 & 0 \\ 0 & \lambda_2 & 0 \\ 0 & 0 & \lambda_3 \end{bmatrix} \begin{pmatrix} \mathbf{v}_1 \\ \mathbf{v}_2 \\ \mathbf{v}_3 \end{pmatrix} \quad (2.9)$$

where \mathbf{D}' is a new tensor while λ_1 , λ_2 , and λ_3 are the eigenvalues and \mathbf{v}_1 , \mathbf{v}_2 , and \mathbf{v}_3 are the eigenvectors that correspond to each λ_1 , λ_2 , and λ_3 , respectively.

The eigenvalues defines the degree of diffusion whereas the eigenvectors illustrates the direction of diffusion in the sense that the largest eigenvector (λ_1) signifies the principle diffusion direction. In case of isotropic diffusion, the eigenvalues are almost equivalent, i.e. $\lambda_1 \approx \lambda_2 \approx \lambda_3$. On the other hand, in condition where the diffusion is anisotropic, the eigenvalues are significantly different, e.g. $\lambda_1 > \lambda_2 > \lambda_3$ (Alexander et al., 2007; Winston, 2012). The diffusion tensor model of isotropic and anisotropic diffusion could be visualized by a sphere and ellipsoid, respectively. In free water, movement of water molecules is unrestricted therefore the diffusion is equal in all directions and characterized by sphere model. In contrast, in

the presence of barrier, mobility of water molecules is restricted thus the diffusion is anisotropic and described by an ellipsoid (Fig. 2.3).

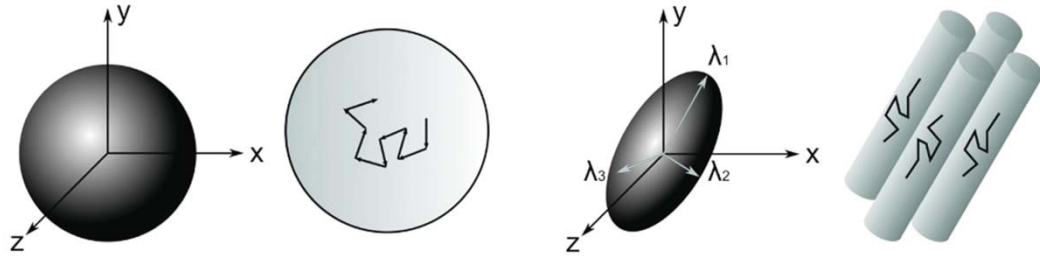


Fig. 2.3 Illustration of isotropic and anisotropic diffusion (Winston, 2012, p. 258).

As ADC of isotropic diffusion (i.e. D in Eq. 2.7) can be estimated through simple linear regression, e.g. least-square fitting (Mori, 2007a), however, estimation of ADC for anisotropic diffusion (i.e. \mathbf{D}' in Eq. 2.9) is performed using multivariate linear regression (Mori, 2007b). This could be achieved by acquiring seven sets of data images i.e. diffusion-weighted images along at least six different directions (measurement in three orthogonal axes) and one b_0 images (Mori, 2007c; Mukerjee et al., 2008a; Basser and Pierpaoli, 1998).

2.3.2 DTI indices

Main advantage of DTI compared to other MR techniques is it provides multiple scalar indices which have the ability to give structural informations at macro- and microscopic scale. Amongst scalar indices derived from DTI include *Trace* (\mathbf{D}), which is the sum of the three eigenvalues λ_1 , λ_2 , and λ_3 . While mean diffusivity (MD) is computed as average of the three eigenvalues λ_1 , λ_2 , and λ_3 or equals to $\frac{1}{3}$ of *Trace* (\mathbf{D}). Both indices describe the average diffusivity of water molecules within a voxel. *Trace* (\mathbf{D}) and MD are characterized by Eq. 2.10 and 2.11:

$$\text{Trace}(\mathbf{D}) = \lambda_1 + \lambda_2 + \lambda_3 \quad (2.10)$$

$$MD = \frac{\text{Trace}(\mathbf{D})}{3} \quad (2.11)$$

Whereas the indices that quantify the directionality of water molecules in a particular voxel are fractional anisotropy (FA) and relative anisotropy (RA), which are represented by Eq. 2.12 and 2.13:

$$FA = \sqrt{\frac{3}{2}} \sqrt{\frac{(\lambda_1 - MD)^2 + (\lambda_2 - MD)^2 + (\lambda_3 - MD)^2}{\lambda_1^2 + \lambda_2^2 + \lambda_3^2}} \quad (2.12)$$

$$RA = \sqrt{\frac{1}{3}} \frac{\sqrt{(\lambda_1 - MD)^2 + (\lambda_2 - MD)^2 + (\lambda_3 - MD)^2}}{MD} \quad (2.13)$$

The indices vary from isotropic diffusion to greatest anisotropy in scale 0 to 1 and 0 to $\sqrt{2}$ for FA and RA , respectively. FA maps are commonly depicted in red, green, and blue (RGB) colour-coded form which represents the main directions of water mobility (thus fibre directions) in a particular voxel. Red, green, and blue indicates diffusion in right-left (R-L), anterior-posterior (A-P), and superior-inferior (S-I) directions, respectively.

Another index is volume ratio (VR) which measures the ratio between ellipsoid volume to sphere volume. Its values vary between 1 (isotropic diffusion) to 0 (largest anisotropy). VR is described by Eq. 2.14:

$$VR = \frac{\lambda_1 \times \lambda_2 \times \lambda_3}{MD^3} \quad (2.14)$$

Quantification of DTI also takes into account of the axial and radial diffusivity which corresponds to λ_1 itself as well as mean of λ_2 , and λ_3 , respectively. The axial diffusivity, D_{\parallel} and radial diffusivity, D_{\perp} (Eq. 2.15) stands for ADC in the direction

parallel and perpendicular to the fibres in each voxel, respectively. Both indices are specific markers for characterizing the condition of axon and myelin of the neuronal fibres (Pierpaoli and Basser, 1996; Song et al., 2002). However, measurement and interpretation of these indices should be complemented by detailed analysis on the mathematical and geometrical properties of the tensor ellipsoids (Wheeler-Kingshott and Cercignani, 2009).

$$D_{\perp} = \frac{\lambda_2 + \lambda_3}{2} \quad (2.15)$$

Among all scalar indices, the most frequently used for general assessment of white matter integrity are *MD* and *FA* (Xiang-qing et al., 2010; Gons et al., 2011; Lochner et al., 2012) while the rest are used for other detailed analysis (Kraus et al., 2007; Chen et al., 2012). An example of DTI parametric maps are shown in Fig. 2.4.

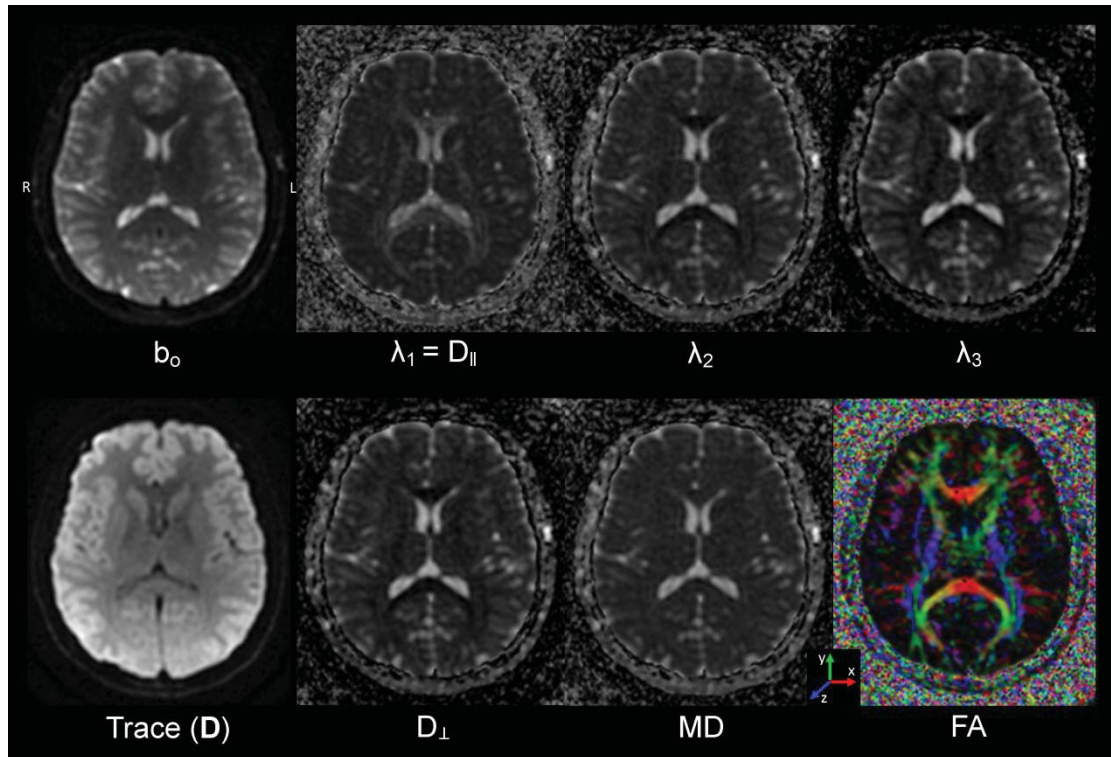


Fig. 2.4 An example of b_0 , principle diffusivities (λ_1 , λ_2 , λ_3), Trace (D), radial diffusivity (D_{\perp}), MD, and colour coded FA maps as obtained from this work.

2.4 Fibre tractography

Besides offering various quantitative informations, DTI also permits visualization of neuronal fibers in three dimensional forms through methods called fiber tractography as obtained from this work and is shown in Fig. 2.5. In Fig. 2.5 fibre tractography is presented according to the standard RGB colour coding scheme of the FA map, as described in Section 2.4.2. Specifically, red, green, and blue denotes neuron fibres in R-L, A-P, and S-I directions, respectively.

Recently, there are two methods used to construct the fiber tracts specifically deterministic (Conturo et al., 1999; Mori et al., 1999) and probabilistic (Parker et al., 2003; Lazar and Alexander, 2003; Jones and Pierpaoli, 2005). The former method is based on line propagation technique in which principle diffusion direction is used to propagate direction for each voxel. The latter method is based on global energy minimization technique. This technique involves a process that find the most probable pathway between two predetermined voxels until it reach a threshold i.e. the minimum allowable tensor anisotropy (Mori and Zijl, 2002; Masutani et al., 2003).

Fiber tractography has opened up new vistas for better understanding of the underlying neural circuitry and interrelationship between various areas in both normal (Dougherty et al., 2007; Nucifora et al., 2007; Johansen-Berg and Rushworth, 2009; Yasmin et al., 2009; Charlton et al., 2010;) and diseased brain (Singh et al., 2010; Shu et al., 2011; Bai et al., 2012; Reijmer et al., 2013).

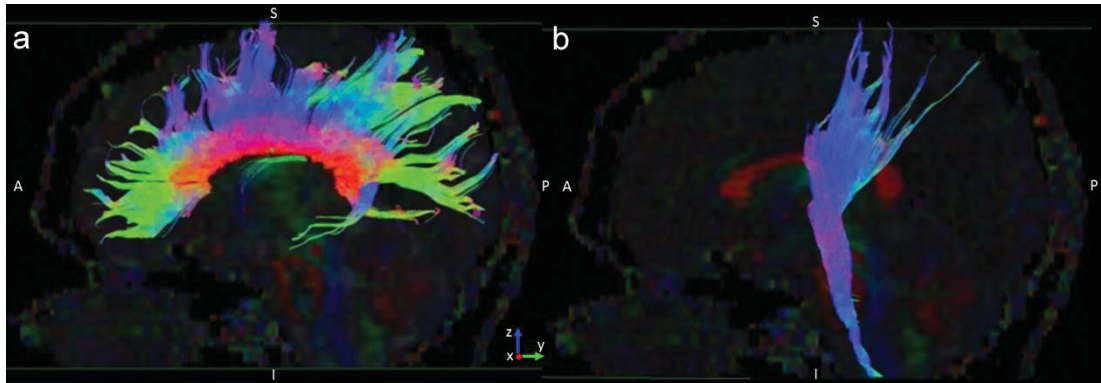


Fig. 2.5 An example of fibre tractography overlaid on colour-coded FA map. The images depict two main fibre bundles in the white matter such as (a) corpus callosum and (b) cerebrosplinal tract from left sagittal view.

2.5 Technical considerations

Since the emergence of DWI in 1980s and followed by DTI in 1990s, it has been used extensively in brain imaging, particularly for white matter studies. However, to date, there is no consensus on the standard imaging protocol employed. Success of performing DTI scan and acquiring quantitative informations from it depends on several important technical aspects:

2.5.1 Trade-offs between resolution, SNR, and scan time

Accuracy of DTI outcome is governed by accurate estimation of diffusion tensor orientation of every voxel. As in general MRI technique, in order to obtain an acceptable image quality, data images must be acquired with the smallest voxel size as possible (i.e. highest spatial resolution) at the same time maintaining acceptable SNR. Such procedure requires extensive time allocations. Moreover, amount of diffusion weighting, which is restricted by echo time (TE) needs to be sufficient as well. Apart from the influence of various image acquisition parameters (Mori, 2007d; Mukherjee et al., 2008b; McRobbie, 2006b), the subjects themselves also had a major influence on the image quality e.g. physiologic motion. Therefore, it is

important to determine the tolerable total scan time for subjects in designing the scanning protocol for each study (Mori, 2007d; Jones et al., 2002).

2.5.2 Diffusion encoding directions

Particular concern should also be given to the number of diffusion gradient directions applied during the scan (Giannelli et al., 2010). At least 20 unique directions was reported necessary for a robust estimation of anisotropy, whereas at least 30 directions are required for a robust estimation of tensor orientation and mean diffusivity (Jones, 2004). It is also recommended from previous work that decision on the number of directions applied should be made based on the objective of each study (Ni et al., 2006). This study thus uses 30 directions in order to obtain the required and sufficient quantitative analysis of DTI maps.

2.5.3 Ratio of DWI: b_0 images

For the best estimates of diffusion orientation, it is also suggested that some sets of b_0 images to be acquired in addition to the DWI, specifically single set of b_0 images for every 5 to 10 sets of DWI and 3 to 6 sets of b_0 images for 30 sets of DWI (Mukherjee et al., 2008b; Alexander and Barker, 2005; Jones et al., 1999a).

2.5.4 Parallel imaging

Besides EPI, other efforts have been made to shorten the scan time i.e. by employing parallel imaging technique. This technique uses spatial information collected by multi-channel receiver coil in which the number of phase encoding steps in the k -space is reduced. This will form “aliasing” artefact in the images due to reduced FOV. Subsequently, “unaliasing” procedure is performed to construct a complete data images (Fig 2.6) (Glockner et al., 2005; Heidemann et al., 2003).

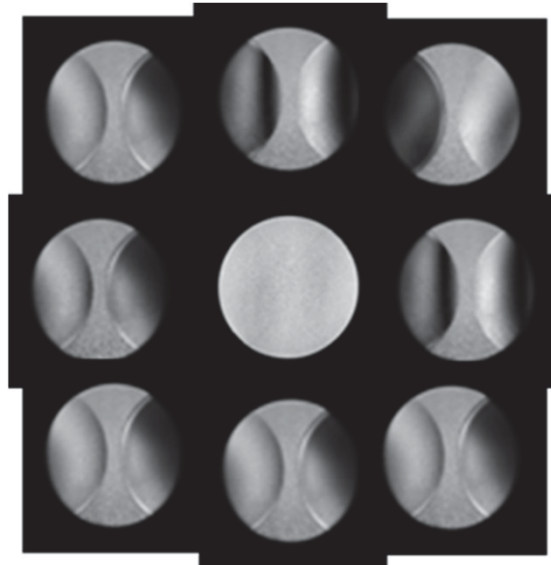


Fig. 2.6 Parallel reconstruction of data in which images with aliasing artefacts are obtained simultaneously. The data are then combined to obtain a complete image (centre) (Clarke, 2007).

2.5.5 Artefacts

It is important to identify some of the artefacts that are commonly associated with DTI. This is because in DTI technique diffusion tensor is calculated for each image voxel. Any defects in the image will give a vast impact on the interpretation of the data and the findings of a study. Below are the some of the most common artefacts found in DTI.

2.5.5 (a) Eddy currents artefact

Rapid switching of strong magnetic field gradient by the gradient coils during data acquisition causes eddy currents induction in the electrical conductor of the MRI scanner. This produces undesirable, rapid and slow decay of magnetic field, thus effect the results in two ways i.e. cause alterations of the field gradients as well as slow decay of the field during data images readout, which then leads to geometrical distortion of the images. Furthermore, DTI scan are most commonly performed using

EPI sequence. Despite of its advantages in reducing scan time, however, EPI is very vulnerable to eddy currents induction which causes significant distortion and misregistration in the DWI (Basser and Jones, 2002).

Besides parallel imaging technique and segmented k -space sampling, post-processing techniques are also most commonly used approach to eliminate or reduce eddy currents artefact (Tournier et al., 2011; Kim et al., 2006; Mangin et al., 2002).

2.5.5 (b) Susceptibility artefact

Large discontinuities in bulk magnetic susceptibility generate local magnetic field gradients that may also cause significant distortion in the DWI. This artefact normally occurs at tissue-air interfaces e.g. region near the sinuses. Single-shot EPI is sensitive to this artefact and it is usually more severe along the phase encoding direction. Furthermore, severity of artefact also correlated linearly with magnetic field strength (Basser and Jones, 2002).

General methods to reduce this artefact include use of multi-shot EPI to reduce the time for image readout and use of parallel imaging technique (Hiwatashi and Zhong, 2005). In addition, other approaches are used as well (Andersson et al., 2003; Merhof et al., 2007).

2.5.5 (c) Motion artefact

Subject motion, either in the form of gross head movement or physiologic motion e.g. eye movement, respiratory motion, and CSF pulsation may also contribute to production of artefact. This is mainly due to spins experiencing considerable phase shifts which will then cause ghosting and high signal variation in an image.

Amongst the possible methods to correct this artefact are by applying phase correction on the data images as well as use of fast imaging technique such as parallel imaging. Besides, use of navigator echo and cardiac gating are also suggested (Basser and Jones, 2002; Hiwatashi and Zhong, 2005; Le Bihan et al., 2006).

2.6 Application of DTI in brain imaging

Until now, DTI is the only imaging technique that allows examination of brain microstructure noninvasively. The parameter indices derived provided various information that permits users to infer the physiological process that take place in human brain, specifically white matter at both macro- and micro-structural level.

Since its introduction, application of DTI in basic clinical research has been vast (Horsfield and Jones, 2002; Zarei et al., 2003; Le Bihan and Johansen-Berg, 2012). This technique has been employed in studying various diseases, such as stroke (Sotak, 2002; Sea Lee et al., 2005; van der Aa et al., 2011), multiple sclerosis (Werring et al., 1999; Hesseltine et al., 2006; Sbardella et al., 2013), brain tumor (Lu et al., 2003; Chen et al., 2012; Abd-El-Barr et al., 2013), as well as Alzheimer's disease (Rose et al., 2000; Zhang et al., 2007; Rowley et al., 2013). Utilization of DTI in the study of psychiatric diseases includes depression (Nobuhara et al., 2006; Li et al., 2007; Liao et al., 2013) and schizophrenia (Burns et al., 2003; Ellison-Wright and Bullmore, 2009).

Besides, DTI technique is also employed in research on assessment of white matter abnormalities particularly leukoaraiosis (O'Sullivan et al., 2004; Jones et al.,

1999b; Qu et al., 2010), which is one of the major items to be discussed in this thesis. A brief explanation on leukoaraiosis is described in the following subsection.

2.6.1 Leukoaraiosis

“Leukoaraiosis” is a general terminology describing white matter lesion seen on brain scan. The term which comes from Greek, *leuko* (white) and *araiosis* (rarefaction), was introduced by Hachinski et al. to express a type of pathological condition in brain white matter (Hachinski et al. 1987). Areas of leukoaraiosis usually appear hypointense in T1-weighted image and hyperintense in T2-weighted and fluid attenuated inversion recovery (FLAIR) image of the white matter area. Leukoaraiosis is commonly found in the elderly and predominantly increases with age (Grueter and Schulz, 2011). It also could be observed in patients with diseases such as cerebral ischemia, dementia, and many other diseases. It was reported that leukoaraiosis could also be a predictor of stroke (Kuller et al., 2004; Smith, 2010).

Leukoaraiosis is associated with age and multiple vascular risk factors such as hypertension, cerebral infarction, diabetes mellitus, as well as ischemic heart disease, as proven by some pathological studies (Zhang and Kang, 2013). Most of the studies on leukoaraiosis are in the field of histopathology, psychiatry, and psychology (Lamar et al., 2007; Simpson et al., 2007; Teodorczuk et al., 2007; Viana-Baptista et al., 2008). Histological findings suggested that leukoaraiosis is associated to axonal loss and progressive glial activation (Pantoni et al., 1997). Neuroimaging studies employing DTI showed higher MD and reduced FA in the leukoaraiosis areas (Jones et al., 1999b; Cercignani et al., 2001; Qu et al., 2010).

CHAPTER 3

FEASIBILITY OF ACQUIRING DTI DATA AND CONSTRUCTING PARAMETRIC MAPS AND FIBRE TRACTOGRAPHY

3.1 Introduction

Besides the ability to provide quantitative information, DTI also differs from the conventional MRI in the aspect of image acquisition. In DTI image acquisition, a set of MR images is acquired with diffusion-weighting applied along many different directions. Application of diffusion-weighting in various directions enables for complete characterization of diffusion in anisotropic systems in the brain (Basser and Jones, 2002).

As DTI imaging was performed for the first time, the feasibility of acquiring DTI data using 1.5 T MRI system was evaluated first before the study on leukoaraiosis was carried out. In this study, the capability of the MRI system to produce results that could distinguish leukoaraiosis from healthy white matter was also evaluated.

3.2 Materials and Methods

3.2.1 Subjects

As a pilot study to look for the feasibility of acquiring DTI data, two healthy male volunteers were recruited. Subject 1 and 2 were 24.2 and 29.7 years old, respectively when the scanning was performed. Then, for comparison between leukoaraiosis and healthy brain, two healthy male volunteers with either occipital leukoaraiosis or